Novel Nanocombinations of L-tryptophan and L-cysteine: Preparation, Characterization and Their Applications for Dye Decolorization, Antimicrobial and Anticancer Activities

Ahmed I. Abd-Elhamid
City of Scientific Research and Technological Applications (SRTA- City), New Borg EL Arab
Hamada El-Gendi
City of Scientific Research and Technological Applications (SRTA- City), New Borg EL Arab
Abdallah E. Abdallah
Al-Azhar University
Esmail El-Fakharany (esmailelfakharany@yahoo.co.uk)
City of Scientific Research and Technological Applications (SRTA- City), New Borg EL Arab

Research Article

Keywords: nanoparticles, two amino acids (AAs) L-tryptophan (Trp) or L-cysteine, Candida albicans

Posted Date: June 24th, 2021

DOI: https://doi.org/10.21203/rs.3.rs-650889/v1

Abstract

Tungsten oxide WO_3 nanoparticles (NPs) were prepared in a form of nanosheets with a homogeneous size and dimensions in one step through acid precipitation using a cation exchange column. The resulting WO_3 nanosheets surface was decorated with one of the two amino acids (AAs) L-tryptophan (Trp) or L-cysteine (Cys) for their dye removal, antimicrobial, and antitumor activities. A noticeable improvement in the biological activity of WO_3 NPs was detected upon amino acid modification compared to the original WO_3. The prepared WO_3-Trp and WO_3-Cys exhibited strong dye removal activity toward methylene blue and safranin dyes with complete dye removal (100%) after 6 h. WO_3-Cys NPs and WO_3-Trp NPs revealed higher broad-spectrum antibacterial activity toward both G-ve and G+ve bacteria with strong antifungal activity toward *Candida albicans*. Anticancer results of the modified WO_3-Cys and WO_3-Trp NPs against various kinds of cancer cells including MCF-7, caco-2, and HepG-2 cells indicated that they have a potent effect in a dose-dependent manner with high selectivity to cancer cells and safety against normal cells. The expression levels of E2F2, Bcl-2 genes were found to be suppressed after treatment with both WO_3-Cys and WO_3-Trp NPs more than 5-FU-treated cells. While expression level of the p53 gene in all tested cells was evidently up-regulated after treatment by more than 5-8 folds as compared to untreated cells. The docking results confirmed the ability of both NPs to bind to P53 gene with relevant potency in binding to other tested gens and participation of cysteine SH-functional group in such interaction.

Introduction

Tungsten oxide (WO_3) is considered as one of the most promising transition metal oxides, for their regard performance in various applications including electrochromic devices [1,2], dye-sensitized solar cells [3,4], photocatalytic applications [5], sensing applications [6,7], field-emission applications [8], high-temperature superconductors [9], optical recording devices [10] and adsorbent [11]. The wide application for WO_3 could be attributed to its high chemical stability and remarkable electric conductivity in addition to the ability to reverse-redox process [12]. Moreover, tungsten oxide could be prepared in different morphologies involved: nanorods [13], nanotubes [14], nanosheets [7], nanowires [15], and nanobelts [16]. Several techniques were investigated for the preparation of WO_3 using either physical or chemical approaches; thermal evaporation [17], spray pyrolysis [18], sol-gels [19], templating method [20], hydrothermal [13], electrochemical anodization [21], electrodeposition [12], microwave-assisted method [5]. however, these methods are time-consuming, and relatively complicated processes with a limitation in controlling the size and shape of the resulted nanoparticles [5,22]. One of the simplest and cost-effective methods for preparing tungsten trioxide nanoparticles is acid precipitation [23]. Great attention is recently directed toward increasing the nanometals implementation in various industrial sectors attributed to its tiny size and large surface-to-mass ratio, besides it's a remarkable stability toward many harsh conditions [24,25]. Nonetheless, the high biotoxicity of some well-known NPs (Ag, Cu, Ti, etc.) restricted their wide commercial usage [26,27]. To overcome the toxicity issue, attention was directed toward NP-oxides as a more safer and effective

alternative [28]. In the same regard, NPs surface modification was also proposed to increase the NPs applicability range with lower side toxicity [29,30]. Recently, growing interest in nanoparticles surface functionalization with different functional groups and bio-macules as amino acids, short peptide, and proteins toward new applications was intensively reported [29,31]. Owing to the large surface-to-mass ratio, NPs adsorb these biomolecules on their large surface area in corona-like structure through Van der Waals forces revealing new biological activity [32].

Nowadays, surface-functionalized NPs are efficiently applied in many fields including environmental and medical ones. With growing dye-dependent industries, synthetic dye effluents represent great environmental and public health challenges attributed to their significant toxicity [25,33–35]. Though many approaches were proposed for dye remediation [33], the lower efficiency and high cost involved limiting their commercial applications [36]. Biotechnological applications of various NPs in hazardous chemicals remediation is an emerging field [25], with advantages of surface modification that greatly enhance their dye-removal capacity [37]. Cancer is recently seen as a global health threat and it consider the world's second leading cause of death, as well as it is expected to become the leading cause of death in the future years [38,39]. Cancer treatment usually resulted in immunosuppression for treated patients, a condition that renders them at high risk for severe microbial infections [40]. Developing a new anticancer agent with consolidated antimicrobial activity is a pressing need. To this end, inorganic nanometals represent one step forward, with their high antitumor and antimicrobial activity with minor bacterial-resistance evolution ability [41]. Moreover, the high stability of NPs toward harsh conditions including temperature and pH intensify the efforts for its successful medical applications [42]. Short peptides and amino acids also attracted attention as promising antimicrobial agents [43]. Currently, a wide interest in the individual AAs' interaction with different NPs for better understanding and elucidation of corona-like structure and give a deeper insight for the new resulting biological activity [44,45]. Cysteine and tryptophan-rich short peptides revealed potent antimicrobial activity against many human pathogens [46,47]. The current study concerning the preparation and functionalization of WO_3 NPs with tryptophan or cysteine amino acids and evaluating the efficacy of the resulted NPs-AAs in versatile applications including synthetic dye removal, antimicrobial, and antitumor activities.

Results And Discussions

Characterization of WO_3 NPs and WO_3-amino acid (WO_3-AAs) complex

The WO_3 NPs was prepared from Na_2WO_4 solution through strong HCl acid type of cation exchange resin. The yielded yellow solution was precipitated and dried at 70°C. The surface of dried NPs was functionalized with Trp or Cys (Fig. 1). The appearance of synthesized $WO_3 \cdot H_2O$ and modified WO_3-AAs at various magnification is explored by SEM (Fig. 2). The SEM photos presented $WO_3 \cdot H_2O$ in separated nanosheets morphology with a homogeneous size and dimensions (Fig. 2). The functionalized WO_3-AAs complexes under the SEM microscope presented as coagulated structure formed from of the $WO_3 \cdot H_2O$

sheets linked with each other by the amino acid to form agglomerated $WO_3.H_2O$ nanosheets/AAs complexes (Fig. 2). In a similar work, individual amino acids, especially for histidine, were proposed for better understanding the NPs and protein interaction [51].Though several mechanisms were proposed for interaction of protein and amino acids on the surface of NPs, the exact mechanism is not fully understood [30]. The crona-like structure resulting upon the proteins and NPs interaction is well stablished theory for elucidating the different biological behavior of NPs in the biological media [51,52]. It importance to note that, the $WO_3 \cdot H_2O$ still keep on its sheet morphology in the resulted WO3-AAs complexes.

Energy-dispersive X-ray spectroscopy (EDS) was applied for revealing the elemental analysis of the materials. The analysis demonstrated that the synthesized $WO_3.H_2O$ is free form impurities (Fig. 2). The analyzed powder is shown to be composed of %At (W = 42.10 and O = 57.90). After modification of WO_3 NPs with Trp or Cys, the EDS analysis of the complexes (WO_3-Trp & WO_3-Cys) showed the presence of carbon, as revealed in Fig. 2, denoting the carbons comes from amino acid.

The FT-IR spectra was used to identify the structural functional groups of $WO_3.H_2O$ and WO_3-AAs complexes (Fig. 3a). The IR spectrum of $WO_3.H_2O$ (Fig. 3a) revealed a broad band at 3387 cm^{-1} corresponding to the stretching motion of (O-H), the band at 1624 cm^{-1} is due to in-plane bending δ(H-O-H) of the water molecule. Moreover, the week band at 938 cm^{-1} characterized the stretching of ($W=O_t$) (where O_t the terminal oxygen). The intense sharp band at 666 cm^{-1} revealed the stretching (W-O). Upon reacting with Trp or Cys, the peaks related to the stretching motion of (O-H) and become more intense, broader and shifted to 3428 and 3442, respectively (Fig. 3a). Furthermore, the bending δ(H-O-H) of the water molecule band become more intense and shifted to 1650 cm^{-1} with Trp and to 1644 cm^{-1} in case of Cys. Moreover, a new bands appears at 1434, 1272, 1115, 1063, 984, 888, 627, 525 cm^{-1} for WO_3-Trp complex and 1423, 1272, 1114, 1061, 983, 888, 654, 532 cm^{-1} for WO_3-Cys complex where the intense sharp band at 666 cm^{-1} disappear (Fig. 3a). These results clearly confirm the successful interaction between the two amino acids and WO_3 NPs.

The thermal stability of $WO_3.H_2O$ and WO_3-AAs complexes were tested using TGA analysis as seen in Fig. 3b. The $WO_3.H_2O$ present two main decomposition stages 64-90^oC (2.5%) related to evaporation of adsorbed water 197-249^oC (4.5%) corresponding to release of intermolecular water (Fig. 3b). Attributed to modification of the WO_3 NPs with tryptophan (WO_3-Trp) or cysteine (WO_3-Cys), the TGA properties of the produced composites highly alter from the original WO_3 (Fig. 3b). For the both composites, desorption of solvent, physically bonded water and surface hydroxyl groups was assessed through the loss in the mass in the region below 200°C. at temperature (≥ 250°C) the two composites presented smoothly decrease in their masses. This is related to the degradation of the organic materials on the substrate of WO_3 NPs (Fig. 3b). This decomposition behavior presented suitable thermal stability for the organic modifier confirming the interaction and linking of the amino acids molecules to the surface of WO_3 NPs.

Dye decolorization activity of prepared WO_3 and modified WO_3-AAs NPs

The ability of modified WO_3-Trp and WO_3-Cys NPs toward synthetic dyes remediation was evaluated against some synthetic dyes solution (100 ppm/final conc.) and compared to plain WO3 NPs and separate AAs. Among the tested dye solutions, WO_3-AAs revealed high dye removal capacity against methylene blue and safranin dyes (Fig. 4) compared to WO_3 NPs and separate AAs. The decolorization rate of the two dyes was further studied through following up dye decolorization for 6 h, where samples were withdrawn and measured using UV-visible spectrophotometer with 1 h interval (Fig. 4). The results indicated great enhancement in the dye removal capacity for WO_3-Trp and WO_3-Cys modified NPs toward methylene blue and safranin dyes with complete dye removal (100%) after 6 h compared to plain WO_3 revealed moderate potential toward two dyes with 47 and 70% of dye decolorization for methylene blue safranin, respectively. The surface modification of WO_3 NP was reported to enhance its dye removal activity [53]. Dinari and his colleagues reported enhancement in methylene blue dye removal by a photocatalytic modified multi-walled carbon nanotube/WO_3 compared to WO_3 NP [54]. The two separate AAs revealed no detectable decolorization activity toward both dyes solution (Fig. 4). Though decolorization rate of WO_3-Trp for both dyes was faster than WO_3-Cys, the time required for complete degradation of methylene blue and safranin dyes was the same (6 h).

Antimicrobial activity of prepared NPs and modified amino acid-NPs

The wide spread for multi-resistance microbial pathogens, implies a necessity for efficient broad spectrum antimicrobial molecules with lower microbial resistance induction capacity. Antimicrobial activity of the WO_3-AAs NPs was investigated against three pathogenic strains including *Staphylococcus aureus* (ATCC 25923), *Pseudomonas aeruginosa* (ATCC 27853), and *Candida albicans* (ATCC 10231) along with plain WO_3 and AAs as controls, refer Table 1. The results (Table 1) indicated that pure WO_3 has no effect on the applied pathogens which in constant to other's findings [53] reported the inability of pure WO_3 to inactivate pathogenic bacterial cells even after under visible light illumination for 6 h. Separate Cys and Trp revealed considerable antimicrobial activity compared to that of Trp and WO_3 NPs**.** The results also indicated a synergistic enhancement in the antimicrobial activity of WO_3 NPs via modification with the applied amino acids as WO_3-Cys revealed higher broad-spectrum antibacterial activity toward *Staphylococcus aureus* and *Pseudomonas aeruginosa* compared to MIC values of Cys (85.82 and 112.7 µg/ml), with limited antifungal activity toward *Candida albicans* (105.9 µg/ml) compared to that of Cys (115 µg/ml). The results are in accordance with other's findings stated the potency of Cys and Cys-rich peptides as promising antibacterial agents [46,55]. Recently, short peptides and amino acids-rich biomolecules rise as promising bacteriostatic agents that most likely targeting outer bacterial membrane rather than intracellular bacterial structures [46,56]. The thiol side chain in cysteine is highly reactive and hypothetically initiate the first interaction toward bacterial cell membranes [46,57]. On the other hand, WO_3-Trp also revealed broad-spectrum antibacterial activity toward *Staphylococcus aureus* (MIC 72.5 µg/ml) and *Pseudomonas aeruginosa* (MIC 104.7 µg/ml) with strong antifungal activity toward *Candida albicans* (42.8 µg/ml). The role of Trp as a hydrophobic AAs in antimicrobial-

peptides was asserted [47,58] through initiating the first and strong anchoring to the bacterial membrane and affect the interface region of lipid bilayer leading to cell membrane destruction.

Anticancer activity of the WO_3 and surface functionalized WO_3-AAs NPs

MTT assay used to determine cell metabolic activity for testing the cytotoxicity of the certain compound or drug. Here in, we evaluated the anticancer effect of the modified WO_3-Trp and WO_3-Cys and NPs against various kinds of cancer cells including MCF-7 caco-2 and HepG-2 cell lines in comparison with free forms of Cys and Trp AAs as well as original WO_3 NPs. Also, we investigated the effect of all of these compounds on WISH cells as a normal cell line. Our results indicated that the highest values of IC_{50} were found to be for normal cells which refer to the highest safety of the applied modified NPs. As presented in table 2, IC_{50} values for of the modified WO_3-Cys and WO_3-Trp NPs against WISH cells were be near of those free forms of Cys, Trp and WO_3 NPs which highlighting their safety.

Furthermore, MCF-7 cells are the most sensitive cells to treatment with both modified NPs. The modified WO_3-Cys NPs had an anticancer activity against MCF-7, Caco-2 and HepG-2 cells after treatment for 48 h at IC_{50} values evaluated to be 92.53±5.2, 162.9±7.5 and 184.5±12.4 µg/ml, respectively, with SI values of 22.01±0.01, 12.49±0.02 and 11.04±0.01, respectively. While after treatment with WO_3-AAs NPs for 48 h, values of IC_{50} were calculated to be 147.5±9.7, 176.3±10.1 and 202.6±15.3 µg/ml against the same cell lines, respectively, with SI values of 14.98±0.03, 12.54±0.02 and 10.91±0.17, respectively. Collectively, the results (Table 2) indicate that WO_3-Cys NPs displayed an anticancer activity higher than WO_3-trp NPs against all tested cells. The interaction of bare NPs to cellular components is indirect [32], where L-cysteine is known to improve the cellular uptake [59], hence, the high activity of the WO_3-Cys NPs may be attributed to the high protonation effect of its SH group to many intracellular proteins [60]. The results are in accordance to [61], demonstrated the role of L-cysteine in suppressing of cancer development through regulating the excess activity of kinases that enhance cancer progression. In addition, a significant increase in the anticancer activity of the modified WO_3-Cys and WO_3-Trp NPs against all tested cancer cells in dose dependent manner with high selectivity to cancer cells and high safety against normal cells (Fig. 5). Fig. 5 also confirms the apoptotic effect of the modified WO_3-AAs NPs and reveals the proportional changes in HepG-2 morphology using nuclear stain method. HepG-2 cells were observed to lose their normal shape after treatment with both modified WO3 NPs for 48 h as compared to reference cells. Fig. 6 also indicates more fragmented HepG-2 chromatin with condensed nuclei in dose dependent manner. Furthermore, all observed chromatin fragmentation, shedding of apoptotic bodies and nuclear condensation were considered the major properties of the apoptotic pathway which became more noticeable with increasing the dose of treatment than untreated cells. Fig. 7 also confirms the effect of the modified WO_3-Cys and WO_3-Trp NPs on expression levels of E2F2, p53 and Bcl-2 genes in MCF-7, Caco-2 and HepG-2 cells as evaluated by real time PCR in comparison with untreated cells as control and 5-fluorouracile (5-FU) treated cells as a standard drug. Fig. 7 indicates that levels of expression of E2F2, Bcl-2 genes were found to be suppressed and down-regulated after treatment with both modified NPs

more than 5-FU-treated cells. Furthermore, expression level of Bcl-2 gene was obviously reduced in the treated cancer cells by around 2 folds more than control cells. While expression level of p53 gene in all tested cells was evidently increased and up-regulated after treatment by more than 5-8 folds as compared to untreated control cells. Collectively, figures 1, 2, and 3 indicated the superiority of modified WO_3-Cys NPs toward all tested cells over that of the modified WO_3-Trp NPs.

Molecular docking studies

Molecular docking studies were carried out for the three compounds into three proteins namely; Bcl-2, P53 and E2F4 which are of crucial roles in cancer development [62–65]. This is to get insights into the proposed targets of the studied compounds and explore to what extent the modified NPs can accommodate the pocket and form interactions with the essential amino acid residues. The crystal structures of the three aforementioned proteins were downloaded from protein data bank (PDB) web site with ID 2W3L, 3ZME and 5TUU, respectively.

For Bcl-2 gene, the obtained results showed the significance of the binding of WO_3-Trp to Bcl-2 through an arene proton interaction with the essential amino acid residue Tyr67 in a manner similar to that of the ligand. Further an arene proton interaction was observed with the side chain of Met74. Additionally, it showed two hydrogen bonds (2.08 and 2.21 Å) with guanidine moiety of Arg105 (Fig. 8a). At the same time WO_3-Cys NPs showed three hydrogen bonds with guanidine moiety of Arg88 (distances, 2.15, 2.16 and 2.40 Å). Moreover, an electrostatic interaction was observed between thiol group of cysteine and alpha proton of Met74 (Fig. 8b). While WO_3 NPs showed four hydrogen bonds with Bcl-2 protein. Two of which were with side chain carboxylate of Glu95 (1.97 and 2.13 Å). The other two were of distances of 2.21 and 3.23 Å with backbone oxygen and mercapto-group of Met74, respectively. With respect to P53 protein, the ligand was found to interact with three residues Asp228, Cys229 and Thr230. The most significant binding pattern with P53 was that of WO_3-Cys NPs which accommodated the pocket showing interactions with the essential residues Cys229 and Thr230 as shown in Fig. 8c. Electrostatic interaction with the beta carbon of Cys229 was observed. Two hydrogen bonds of 1.83 and 2.50 Å length were formed with side chain OH and backbone NH of Thr230, respectively. Additionally, it showed electrostatic interaction with alkyl side chain of Leu145. The second most promising interaction with P53 was that of WO_3 NPs showing a hydrogen bond (distance: 2.26 Å) with the side chain OH of the essential residue Thr230. Moreover, electrostatic interaction with the backbone oxygen of the effective residue Asp228 was observed. Further hydrogen bond (distance: 2.46 Å) was formed with the backbone oxygen of Val147 (Fig. 8d). On the other side the modified WO_3-Trp was unable to accommodate the pocket of P53, showing different binding mode rather than the ligand. However, it formed one hydrogen bond with Thr150 and another with Pro151. It also showed arene proton interactions with Thr150, Pro222 and Pro223.

Finally, E2F4 protein was reported to have four domains; DNA binding domain, a dimerization domain, a transactivation domain, and a pocket protein binding domain [66]. The amino acid residues from 86 to 195

construct dimerization domain. These residues are responsible for formation of heterodimers with a DP family protein [66]. 5TUU at PDB web site is the crystal structure of E2F4-DP1 coiled coil. Docking results into this protein showed three hydrogen bonds for WO_3-Trp NPs as illustrated in Fig. 8e. The first (distance: 2.65 Å) was with guanidine moiety of Arg158. The second was of 2.21 Å length with the backbone oxygen of Ser135. The third one (distance: 2.28 Å) was observed with the backbone oxygen of Thr129. Moreover, an arene proton interaction was formed with Ala138. Regarding WO_3-Cys composite, Fig. 8f shows four hydrogen bonds, two of which were of 2.07 and 2.17 Å lengths with guanidine moiety of Arg158. Another hydrogen bond (2.19 Å length) can be observed with the backbone oxygen of Ala159. The fourth one was of 3.14 Å length with the backbone NH of Ala159. WO_3 NPs showed one hydrogen bond (2.01 Å length) with side chain OH of Thr163. It also showed another hydrogen bond of 2.01 Å length with the backbone oxygen of Ala159.

Material And Methods

Preparation of WO_3 NPs

The WO_3 NPs was prepared by passing 10 ml (0.5M) of Na_2WO_4 (Sigma-Aldrich > 98%) solution through Ion exchanger Dowex® 50 WX 4 (strongly acidic cation exchanger), H form, (obtained from Merck) packed column. The yielded yellow solution was collected from the column using elution process in a blue capped bottle. Thereafter, the bottle placed in oven at 50°C over a period 24 h (Scheme 1: A). The produced precipitate separated by filtration, washed several times with water, dried at 70°C and finally, stored in dark bottle for further use.

Surface functionalized of WO_3 NPs with Tryptophan or cysteine

Surface functionalization of prepared WO_3 was conducted through mixing equal volumes of the prepared WO3 NPs (0.2 mg/ml) with tryptophan or cysteine (0.05 mg/ml) in 0.1 M phosphate pH 7.0 with stirring for 6 h. The mixtures were then centrifuged to eliminate the unbound amino acids, and the resulting NP-AA pellets were used during following experiments (Scheme 1: B).

Characterizations of WO_3 NPs and surface functionalized WO_3-AAs

The pristine WO_3 and surface functionalized WO_3-AAs were characterized using scanning electron microscopy (SEM; JSM 6360LA, Japan), Fourier transform infrared (FT-IR) analysis using Shimadzu FTIR (Model, FTIR8400, Japan), Thermal gravimetric analysis (TGA) (Shimadzu Thermal Gravimetric Analysis (TGA)—50), Japan), and the elemental EDS unit related to SEM.

Application of WO_3 NPs and functionalized WO_3-AAs in synthetic dye removal

The ability of modified WO_3-AAs in synthetic dyes remediation was evaluated against some synthetic dyes solution and compared to plain WO_3 NPs and separate amino acids. Dye solution (100 ppm/final

conc.) were prepared by dissolving methylene blue and safranin in 0.1 M phosphate buffer, pH 7.0. Dye decolorization test was performed in a final volume of 5.0 ml by separately adding 0.4 mg/ml of NPs, WO3-AAs, or AAs to each dye solution. The reaction mixtures were incubated at room temperature for 6 h. Samples were withdrawn from each tube every 1 h and measured using UV-vis spectrophotometer at wavelength of 662 nm and 495 nm for methylene blue and safranin, respectively.

Antimicrobial efficacy of the surface functionalized WO_3-AA NPs

Antimicrobial activity of the prepared WO_3-AA NPs was investigated against three pathogenic strains including *Staphylococcus aureus* (ATCC 25923), *Pseudomonas aeruginosa* (ATCC 27853), and *Candida albicans* (ATCC 10231) along with plain WO_3 and separate AAs as controls. Microplate reader assay was applied in this test where, pre-culture was prepared by overnight cultivation of the three organisms on nutrient broth medium at 37°C. Flat-bottom 96 well tissue culture plate wells were inoculated separately with 100 µl of diluted tested organism (10^6 CFU/ml), and serially diluted compounds (5-80 µg) to a final volume of 200 µl. The microtiter plate was incubated overnight at 37°C, and measured at 600 nm with microplate reader. Antimicrobial results were expressed as minimum inhibitory concentration (MIC), defined as the lowest concentration that completely eliminated all cells.

In vitro anticancer studies; Cell culture and media

Human normal amnion (WISH), human cells derived from breast adenocarcinoma (MCF-7), human epithelial derived from colorectal adenocarcinoma (Caco-2), and human hepatocyte carcinoma (HepG-2) cell lines were obtained from (VACSERA, Cairo, Egypt). DMEM and RPMI-1640 media were obtained from (Lonza Lmd. Co., USA). Human WISH and Caco-2 cell lines were cultured in DMEM media supplemented with 10% FBS (Fatal bovine serum). However, MCF-7 and HepG-2 cell lines were cultured in RPMI-1640 media supplemented with 10% FBS.

Cytotoxicity evaluation using MTT assay

The anticancer effect of the functionalized WO_3-AAs NPs was evaluated through MTT (3-[4, 5-Dimethylthiazol]-2, 5-Diphenyltetrazolium bromide) assay protocol using normal and cancerous cells as described previously by El-Fakharany et al. (2020). Briefly, both normal and cancer cells (1.0×10^4/well) were seeded in four sterile 96-well microplates and incubated for 24 h with complete culture media. Serially diluted functionalized WO_3-AAs NPs at concentrations of 0.1-0.5 mg/ml was added to the cultured cells in triplicates and incubated for 48 h in 5% CO_2 incubator. Then, cells were washed 3 times with fresh media and 200 µl of MTT solution (0.5 mg/ml) was added to each well for 3-5 h. After incubation period, MTT solution was substituted with 200 µl of DMSO for dissolving formazan crystals. The optical density was measured at 590 nm using a micro-plate reader. The IC_{50} value (half maximal inhibitory concentration) of each WO_3-AAs NPs that cause killing of 50% cells was determined by the Graphpad Instate software 6.0 and values of selectivity index (SI) which defined as the ratio of IC_{50} of

normal cells versus cancer cells was estimated also as described previously by Abu-Serie and El-Fakharany (2017).

Nuclear staining

The anticancer and apoptotic effect of the WO_3-Cys and WO_3-Trp NPs against HepG-2 cells was studied by fluorescent nuclear stain method using propidium iodide (PI) dye in comparison with untreated reference cells. HepG-2 cells were incubated in triplicates and treated with different NPs at different concentrations of 0.1, 0.2, and 0.3 mg/ml as aforementioned described. Both untreated and treated cells were washed 3 times with fresh media for removing debris and dead cells and then fixed with 4% paraformaldehyde for 10 min at room temperature. After fixing step, permeabilization the cells with 0.5% Triton X-100 and 3% paraformaldehyde was performed for 1 min. The PI dye at concentration of 10 µg/ml was added for staining the cells 20 min. The cells were observed and imaged by a fluorescence phase contrast microscope (Olympus, Japan) using an excitation filter of 480/30 nm [49].

Effect of the prepared WO_3-AA NPs on gene expression

The effect of the prepared WO_3 and WO_3-AA NPs on the expression level of some tumor genes including transcription factor 2 gene (E2F2), tumor suppressor gene (p53) and oncogene (Bcl-2) was determined in human MCF-7, Caco-2 and HepG-2 cells using qPCR method. After treatment the cancer cells with the modified WO_3-Cys and WO_3-Trp NPs at IC_{50} concentrations for each modified NPs as described above, total RNAs of each untreated and treated cancer cell line were extracted using protocol of Gene JET RNA Purification Kit (Thermo Scientific, USA). Real time PCR of each cDNA was carried out by master mix of SYBR green kit using specific primers (Forward/Reverse) as follow: 5’-GCATCCAGTGGAAGGGTGTG-3'/ 5’-ACGTTCCGGATGCTCTGCT-3' for E2F2 gene, 5'-TAACAGTTCCTGCATGGGCGGC-3'/ 5'-AGGACAGGCACAAACACGCACC-3' for p53 gene, and 5'-TCCGATCAGGAAGGCTAGAGTT-3'/ 5'-TCGGTCTCCTAAAAGCAGGC-3' for Bcl-2 gene. The change of the gene expression level for each cell line after and before treatment was determined by using equation of 2-ΔΔCT.

Docking studies

Molecular docking studies were carried out for simulating the interaction of WO_3 NPs and WO_3-AAs into three important cancer developing proteins namely; Bcl-2, P53 and E2F4. The crystal structures of the three aforementioned proteins were downloaded from protein data bank (PDB) web site with ID 2W3L, 3ZME and 5TUU, respectively. Molecular operating environment (MOE) software was used to conduct molecular docking. The downloaded protein was prepared by 3D protonation, deletion of water molecules and unwanted peptide chains and energy minimization. The pocket was obtained by isolation the molecular surface around the binding site (within 4.5 Å near the ligand atom). Validation was carried out by redocking the crystallized ligand. Rigid protocol docking (default protocol) was selected. The docking protocol is considered to be valid when RMSD of the docking pose compared to the co crystal ligand position is about 1.5 Å or less. To prepare WO_3 NPs and modified WO_3-AAs for docking the structure of

the studied compound was built on MOE. 3D protonation was selected then energy minimization (force field: MMFF94x) was applied. The prepared compounds were added to the created database which was then selected for docking according to the default protocol in which the bond rotation method generated ligand conformations. The conformers are placed in the site with the Triangle Matcher method [50].

Statistical Analysis

All data were expressed as mean±SEM (standard error of the mean) of three different experiments measurements. The statistical significance was assessed by the multiple comparisons Tukey post-hoc analysis of variance (ANOVA) using SPSS16 program. Differences of the results were considered statistically significant at (p)-values < 0.05.

Conclusions

Tungsten oxide (WO_3) represents one of the most interesting metal oxide with various potentials industrial application. In this work WO_3 nanosheets were prepared in one single step through cation exchange column and characterized through different methods. The surface modification of the prepared WO_3 NPs with either L-tryptophan or L-cysteine greatly enhanced their biological activities. The prepared WO_3-Trp and WO_3-Cys exhibited strong dye removal activity toward methylene blue and safranin dyes with complete dye removal (100%) after 6 h. The antimicrobial activity assessment revealed broad-spectrum antimicrobial activity toward the three applied organisms *Staphylococcus aureus* and *Pseudomonas aeruginosa,* and *Candida albicans* with higher antibacterial activity from WO_3-Cys and potent antifungal activity through WO3+Trp. The results also indicated a remarkable antitumor activity in a dose-dependent manner through WO_3-Trp and WO_3-Cys toward all applied tumor cell lines (MCF-7, Caco-2, and HepG-2) attributed to induction of apoptotic effects. The highest antitumor activity was against the breast cancer tumor cell MCF-7. WO_3-Cys revealed the superior antitumor activity which could attributed to high activity of the thiol group as indicated in the molecular docking studies. Collectively, the surface modification of WO_3 NPs with amino acids specially that of L-tryptophan or L-cysteine greatly enhanced their biological activities and may expand their industrial applications.

Declarations

Funding

This study did not receive any specific grant from funding agencies in the public, commercial, or not-for-profit sectors.

Author Contributions

All authors have equally contributed to designing and accomplishing the experiments, analyzing and interpreting the results as well as writing and revising the manuscript.

Ethical statement

This research did not include any human subjects and animal experiments.

Competing Interests

The authors declare that they have no competing interests.

References

1. Yang, M., Shrestha, N. K. & Schmuki, P. Thick porous tungsten trioxide films by anodization of tungsten in fluoride containing phosphoric acid electrolyte. *Electrochemistry Communications* **11**, 1908–1911 (2009).

2. Lee, S. H. *et al.* Crystalline WO3 nanoparticles for highly improved electrochromic applications. *Advanced Materials* **18**, 763–766 (2006).

3. Qi, H. *et al.* Triple-layered nanostructured WO3 photoanodes with enhanced photocurrent generation and superior stability for photoelectrochemical solar energy conversion. *Nanoscale* **6**, 13457–13462 (2014).

4. Prabhu, N., Agilan, S., Muthukumarasamy, N. & Senthil, T. S. Enhanced photovoltaic performance of WO3 nanoparticles added dye sensitized solar cells. *Journal of Materials Science: Materials in Electronics* **25**, 5288–5295 (2014).

5. Li, J. *et al.* Microwave-assisted growth of WO3·0.33H2O micro/nanostructures with enhanced visible light photocatalytic properties. *CrystEngComm* **15**, 7904–7913 (2013).

6. Li, J., Liu, X., Cui, J. & Sun, J. Hydrothermal synthesis of self-assembled hierarchical tungsten oxides hollow spheres and their gas sensing properties. *ACS Applied Materials and Interfaces* **7**, 10108–10114 (2015).

7. Wang, C., Li, X., Feng, C., Sun, Y. & Lu, G. Nanosheets assembled hierarchical flower-like WO3 nanostructures: Synthesis, characterization, and their gas sensing properties. *Sensors and Actuators, B: Chemical* **210**, 75–81 (2015).

8. Zhou, J. *et al.* Three-dimensional tungsten oxide nanowire networks. *Advanced Materials* **17**, 2107–2110 (2005).

9. Slimani, Y. *et al.* Improvement of flux pinning ability by tungsten oxide nanoparticles added in YBa 2 Cu 3 O y superconductor. *Ceramics International* **45**, 6828–6835 (2019).

10. Suda, Y., Kawasaki, H., Ohshima, T. & Yagyuu, Y. Characteristics of tungsten oxide thin films prepared on the flexible substrates using pulsed laser deposition. *Thin Solid Films* **516**, 4397–4401

(2008).

11. Park, S. M. & Nam, C. Dye-adsorption properties of WO3 nanorods grown by citric acid assisted hydrothermal methods. *Ceramics International* **43**, 17022–17025 (2017).

12. Zhuzhelskii, D. V. *et al.* Insights on the electrodeposition mechanism of tungsten oxide into conducting polymers: Potentiostatic vs. potentiodynamic deposition. *Synthetic Metals* **267**, 116469 (2020).

13. Sun, Q. *et al.* Hydrothermal synthesis of WO3 nanorods and their performance in the adsorption of Rhodamine B and the synthesis of adipic acid. *Ceramics International* **40**, 11447–11451 (2014).

14. Wang, Z., Zhou, S. & Wu, L. Preparation of rectangular WO3-H2O nanotubes under mild conditions. *Advanced Functional Materials* **17**, 1790–1794 (2007).

15. Lu, N., Yang, C., Liu, P. & Su, X. Preparation of 2 nm tungsten oxide nanowires based on two-phase strategy and their ultra-sensitive NO2 gas sensing properties. *Journal of Colloid and Interface Science* **557**, 311–317 (2019).

16. Hu, X., Ji, Q., Hill, J. P. & Ariga, K. Large-scale synthesis of WOx-EDA nanobelts and their application as photoswitches. *CrystEngComm* **13**, 2237–2241 (2011).

17. Garcia, I. T. S. *et al.* Multifaceted tungsten oxide films grown by thermal evaporation. *Surface and Coatings Technology* **283**, 177–183 (2015).

18. Ji, R. *et al.* Low-temperature preparation of tungsten oxide anode buffer layer via ultrasonic spray pyrolysis method for large-area organic solar cells. *Materials* **10**, (2017).

19. Au, B. W. C., Chan, K. Y., Pang, W. L., Lee, C. L. & Mustafa, A. H. Tungsten oxide (Wo3) films prepared by sol-gel spin-coating technique. *Solid State Phenomena* **280 SSP**, 71–75 (2018).

20. Sadakane, M. *et al.* Preparation of nano-structured crystalline tungsten(VI) oxide and enhanced photocatalytic activity for decomposition of organic compounds under visible light irradiation. *Chemical Communications* **1**, 6552–6554 (2008).

21. Das, P. K. *et al.* Functional Blocking Layer of Twisted Tungsten Oxide Nanorod Grown by Electrochemical Anodization for Photoelectrochemical Water Splitting. *Journal of The Electrochemical Society* **167**, 066501 (2020).

22. Hidayat, D., Purwanto, A., Wang, W. N. & Okuyama, K. Preparation of size-controlled tungsten oxide nanoparticles and evaluation of their adsorption performance. *Materials Research Bulletin* **45**, 165–173 (2010).

23. Nagyné-Kovács, T. *et al.* Effect of pH in the hydrothermal preparation of monoclinic tungsten oxide. *Journal of Solid State Chemistry* **281**, 1–7 (2020).

24. Jamal, M. *et al.* Development of Tungsten Oxide Nanoparticle Modified Carbon Fibre Cloth as Flexible pH Sensor. *Scientific Reports* **9**, 1–9 (2019).

25. Panda, S. K. *et al. Magnetite nanoparticles as sorbents for dye removal: a review*. *Environmental Chemistry Letters* (Springer International Publishing, 2021). doi:10.1007/s10311-020-01173-9

26. Cronholm, P. *et al.* Intracellular uptake and toxicity of Ag and CuO nanoparticles: A comparison between nanoparticles and their corresponding metal ions. *Small* **9**, 970–982 (2013).

27. Agnihotri, R., Gaur, S. & Albin, S. Nanometals in Dentistry: Applications and Toxicological Implications—a Systematic Review. *Biological Trace Element Research* **197**, 70–88 (2020).

28. Baek, Y.-W. & An, Y.-J. Microbial toxicity of metal oxide nanoparticles (CuO, NiO, ZnO, and Sb2O3) to Escherichia coli, Bacillus subtilis, and Streptococcus aureus. *The Science of the total environment* **409**, 1603–1608 (2011).

29. Miller, P. J. & Shantz, D. F. Covalently functionalized uniform amino-silica nanoparticles. Synthesis and validation of amine group accessibility and stability. *Nanoscale Advances* **2**, 860–868 (2020).

30. EL-Fakharany, E. M., Abd-Elhamid, A. I. & El-Deeb, N. M. Preparation and characterization of novel nanocombination of bovine lactoperoxidase with Dye Decolorizing and anti-bacterial activity. *Scientific Reports* **9**, (2019).

31. Havaldar, D. V. *et al.* Differently synthesized gold nanoparticles respond differently to functionalization with L-amino acids. *Particuology* **52**, 97–104 (2020).

32. Saptarshi, S. R., Duschl, A. & Lopata, A. L. Interaction of nanoparticles with proteins: Relation to bio-reactivity of the nanoparticle. *Journal of Nanobiotechnology* (2013). doi:10.1186/1477-3155-11-26

33. Sarkar, S. *et al.* Green polymeric nanomaterials for the photocatalytic degradation of dyes: a review. *Environmental Chemistry Letters* **18**, 1569–1580 (2020).

34. El-Fakharany, E. M. Nanoformulation of lactoferrin potentiates its activity and enhances novel biotechnological applications. *International Journal of Biological Macromolecules* **165**, (2020).

35. El-Fakharany, E. M. Nanoformulation approach for improved stability and efficiency of lactoperoxidase. *Preparative Biochemistry and Biotechnology* **0**, 1–13 (2020).

36. Jiang, T. *et al.* Carbon nanotubes/TiO2 nanotubes composite photocatalysts for efficient degradation of methyl orange dye. *Particuology* **11**, 737–742 (2013).

37. Marcelo, L. R., de Gois, J. S., da Silva, A. A. & Cesar, D. V. *Synthesis of iron-based magnetic nanocomposites and applications in adsorption processes for water treatment: a review*. *Environmental Chemistry Letters* (Springer International Publishing, 2020). doi:10.1007/s10311-020-01134-2

38. Harding, M. C. *et al.* Transitions From Heart Disease to Cancer as the Leading Cause of Death in US States, 1999-2016. *Preventing chronic disease* **15**, E158 (2018).

39. Siegel, R. L., Miller, K. D. & Jemal, A. Cancer statistics, 2020. *CA: A Cancer Journal for Clinicians* **70**, 7–30 (2020).

40. Holland, T., Fowler, V. G. & Shelburne, S. A. Invasive gram-positive bacterial infection in cancer patients. *Clinical Infectious Diseases* **59**, S331–S334 (2014).

41. Aydin Sevinç, B. & Hanley, L. Antibacterial activity of dental composites containing zinc oxide nanoparticles. *Journal of biomedical materials research. Part B, Applied biomaterials* **94**, 22–31 (2010).

42. Tang, Z. X. & Lv, B. F. MgO nanoparticles as antibacterial agent: Preparation and activity. *Brazilian Journal of Chemical Engineering* **31**, 591–601 (2014).

43. Feng, X. *et al.* The Critical Role of Tryptophan in the Antimicrobial Activity and Cell Toxicity of the Duck Antimicrobial Peptide DCATH. *Frontiers in Microbiology* **11**, 1–14 (2020).

44. Costa, D., Savio, L. & Pradier, C. M. Adsorption of Amino Acids and Peptides on Metal and Oxide Surfaces in Water Environment: A Synthetic and Prospective Review. *Journal of Physical Chemistry B* **120**, 7039–7052 (2016).

45. Ustunol, I. B., Gonzalez-Pech, N. I. & Grassian, V. H. pH-dependent adsorption of α-amino acids, lysine, glutamic acid, serine and glycine, on TiO2 nanoparticle surfaces. *Journal of Colloid and Interface Science* **554**, 362–375 (2019).

46. Tsai, Y. C., Tang, C. C., Wu, H. H., Wang, Y. S. & Chen, Y. F. Antibacterial Activity of Cysteine-Derived Cationic Dipeptides. *International Journal of Peptide Research and Therapeutics* **26**, 1107–1114 (2020).

47. Bi, X., Wang, C., Ma, L., Sun, Y. & Shang, D. Investigation of the role of tryptophan residues in cationic antimicrobial peptides to determine the mechanism of antimicrobial action. *Journal of Applied Microbiology* **115**, 663–672 (2013).

48. Abu-Serie, M. M. & El-Fakharany, E. M. Efficiency of novel nanocombinations of bovine milk proteins (lactoperoxidase and lactoferrin) for combating different human cancer cell lines. *Scientific Reports* (2017). doi:10.1038/s41598-017-16962-6

49. El-Fakharany, E. M. *et al.* The Use of Human, Bovine, and Camel Milk Albumins in Anticancer Complexes with Oleic Acid. *Protein Journal* (2018). doi:10.1007/s10930-018-9770-1

50. Abdallah, A. E. *et al.* Design, synthesis and molecular modeling of new quinazolin-4(3H)-one based VEGFR-2 kinase inhibitors for potential anticancer evaluation. *Bioorganic Chemistry* **109**, 104695 (2021).

51. Mudunkotuwa, I. A. & Grassian, V. H. Histidine adsorption on TiO2 nanoparticles: An integrated spectroscopic, thermodynamic, and molecular-based approach toward understanding nano-bio interactions. *Langmuir* **30**, 8751–8760 (2014).

52. Mahmoudi, M. *et al.* Protein− nanoparticle interactions: opportunities and challenges. *Chemical reviews* **111**, 5610–5637 (2011).

53. Jeevitha, G., Abhinayaa, R., Mangalaraj, D. & Ponpandian, N. Tungsten oxide-graphene oxide (WO3-GO) nanocomposite as an efficient photocatalyst, antibacterial and anticancer agent. *Journal of Physics and Chemistry of Solids* **116**, 137–147 (2018).

54. Dinari, M., Momeni, M. M. & Ahangarpour, M. Efficient degradation of methylene blue dye over tungsten trioxide/multi-walled carbon nanotube system as a novel photocatalyst. *Applied Physics A: Materials Science and Processing* **122**, 1–9 (2016).

55. Liu, Y. *et al.* Cysteine potentiates bactericidal antibiotics activity against gram-negative bacterial persisters. *Infection and Drug Resistance* **13**, 2593–2599 (2020).

56. Epand, R. M., Walker, C., Epand, R. F. & Magarvey, N. A. Molecular mechanisms of membrane targeting antibiotics. *Biochimica et Biophysica Acta - Biomembranes* **1858**, 980–987 (2016).

57. Du, X. *et al.* Polylysine and cysteine functionalized chitosan nanoparticle as an efficient platform for oral delivery of paclitaxel. *Carbohydrate Polymers* **229**, 115484 (2020).

58. Chan, D. I., Prenner, E. J. & Vogel, H. J. Tryptophan- and arginine-rich antimicrobial peptides: Structures and mechanisms of action. *Biochimica et Biophysica Acta - Biomembranes* **1758**, 1184–1202 (2006).

59. Wu, S. Y. *et al.* Amino acid-modified PAMAM dendritic nanocarriers as effective chemotherapeutic drug vehicles in cancer treatment: A study using zebrafish as a cancer model. *RSC Advances* **10**, 20682–20690 (2020).

60. Borenfreund, E. & Puerner, J. A. A simple quantitative procedure using monolayer cultures for cytotoxicity assays (HTD/NR-90). *Journal of Tissue Culture Methods* **9**, 7–9 (1985).

61. Kato, M. *et al.* L-cysteine as a regulator for arsenic-mediated cancer-promoting and anti-cancer effects. *Toxicology in Vitro* **25**, 623–629 (2011).

62. Gascoyne, R. D. *et al.* Prognostic significance of Bcl-2 protein expression and Bcl-2 gene rearrangement in diffuse aggressive non-Hodgkin's lymphoma. *Blood* **90**, 244–251 (1997).

63. Bodner, S. M. *et al.* file:///E:/2020 work/Ahmed Ibrahem work/new witing on WO3 with results/returned from Esmail with molecular docking/refrence 4 molecular docking.pdf. *Oncogene* **7**, 743–749 (1992).

64. Garneau, H., Paquin, M. C., Carrier, J. C. & Rivard, N. E2F4 expression is required for cell cycle progression of normal intestinal crypt cells and colorectal cancer cells. *Journal of Cellular Physiology* **221**, 350–358 (2009).

65. Joensuu, H., Pylkkänen, L. & Toikkanen, S. Bcl-2 protein expression and long-term survival in breast cancer. *American Journal of Pathology* **145**, 1191–1198 (1994).

66. Hsu, J. & Sage, J. Novel functions for the transcription factor E2F4 in development and disease. *Cell Cycle* **15**, 3183–3190 (2016).

Tables

Table 1. The antimicrobial activity (MIC values) of the modified WO_3-Cys and WO_3-Trp NPs against three pathogenic microorganisms in comparison with WO_3 NPs and free amino acids (Cys and Trp).

Test organism	WO_3	WO_3-Trp	WO_3-Cys	Trp	Cys
Staphylococcus aureus	452.90	72.53	53.14	454.00	85.82
Pseudomonas aeruginosa	307.70	104.70	60.52	199.50	112.70
Candida albicans	324.90	42.81	105.90	199.50	115.00

Table 2. EC_{100}, IC_{50} (µg/mL) and SI values of the modified WO_3-Cys and WO_3-Trp NPs against WISH, MCF-7, Caco-2 and HepG-2 cell lines after treatment for 48 h in comparison with WO_3 NPs and free amino acids (Cys and Trp).

All values were expressed as mean ± SEM.

Figures

Sample		WISH	MCF-7	Caco-2	HepG-2
WO_3	IC_{50}	2315±224.3	2805±196.6	2238±210.4	2517±232.5
	SI	-	0.83±0.08	1.03±0.09	0.92±0.1
Cys	IC_{50}	2221±159.8	2365±159.7	2635±118.9	2936±102.1
	SI	-	0.94±0.07	0.84±0.05	0.76±0.04
Try	IC_{50}	2064±197.5	2210±156.9	2084±188.4	2958±134.7
	SI	-	0.93±0.07	0.99±0.09	0.69±0.06
WO_3-Cys	IC_{50}	2036±193.2	92.53±5.2	162.9±7.5	184.5±12.4
	SI	-	22.01±0.01	12.49±0.02	11.04±0.01
WO_3-Trp	IC_{50}	2210±166.8	147.5±9.7	176.3±10.1	202.6±15.3
	SI	-	14.98±0.03	12.54±0.02	10.91±0.17

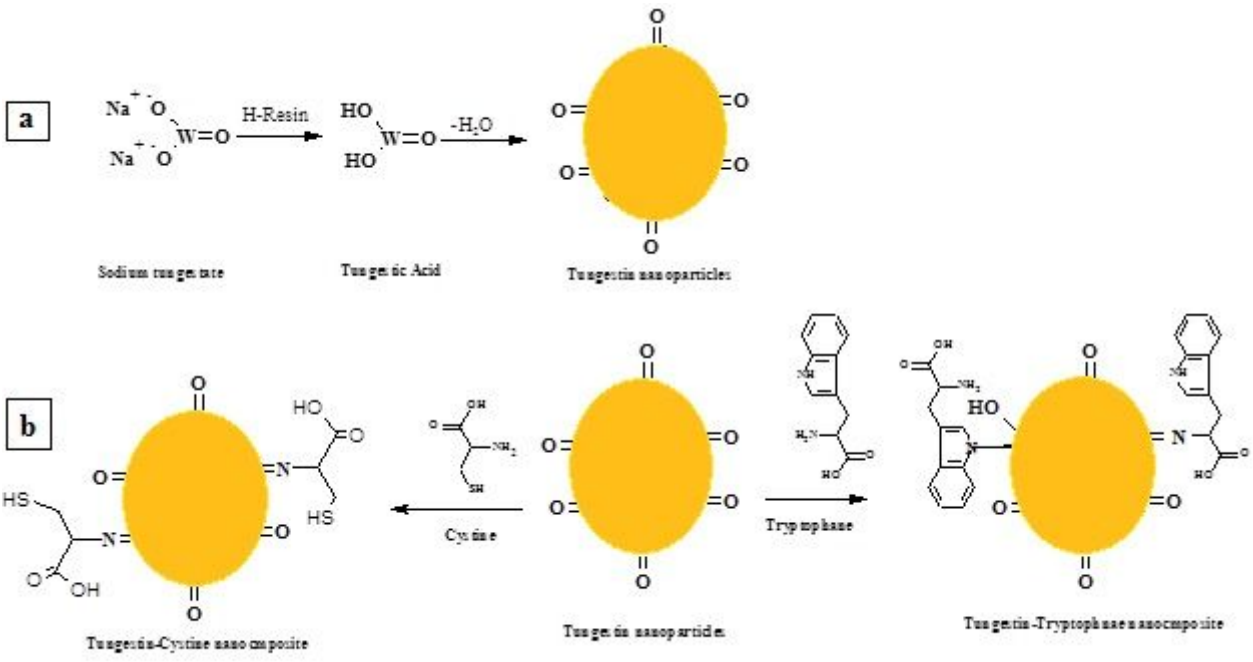

Figure 1

Preparation of WO3 NPs through cation resin (a) and interaction of the prepared WO3 NPs with L-tryptophan or L-cysteine (b).

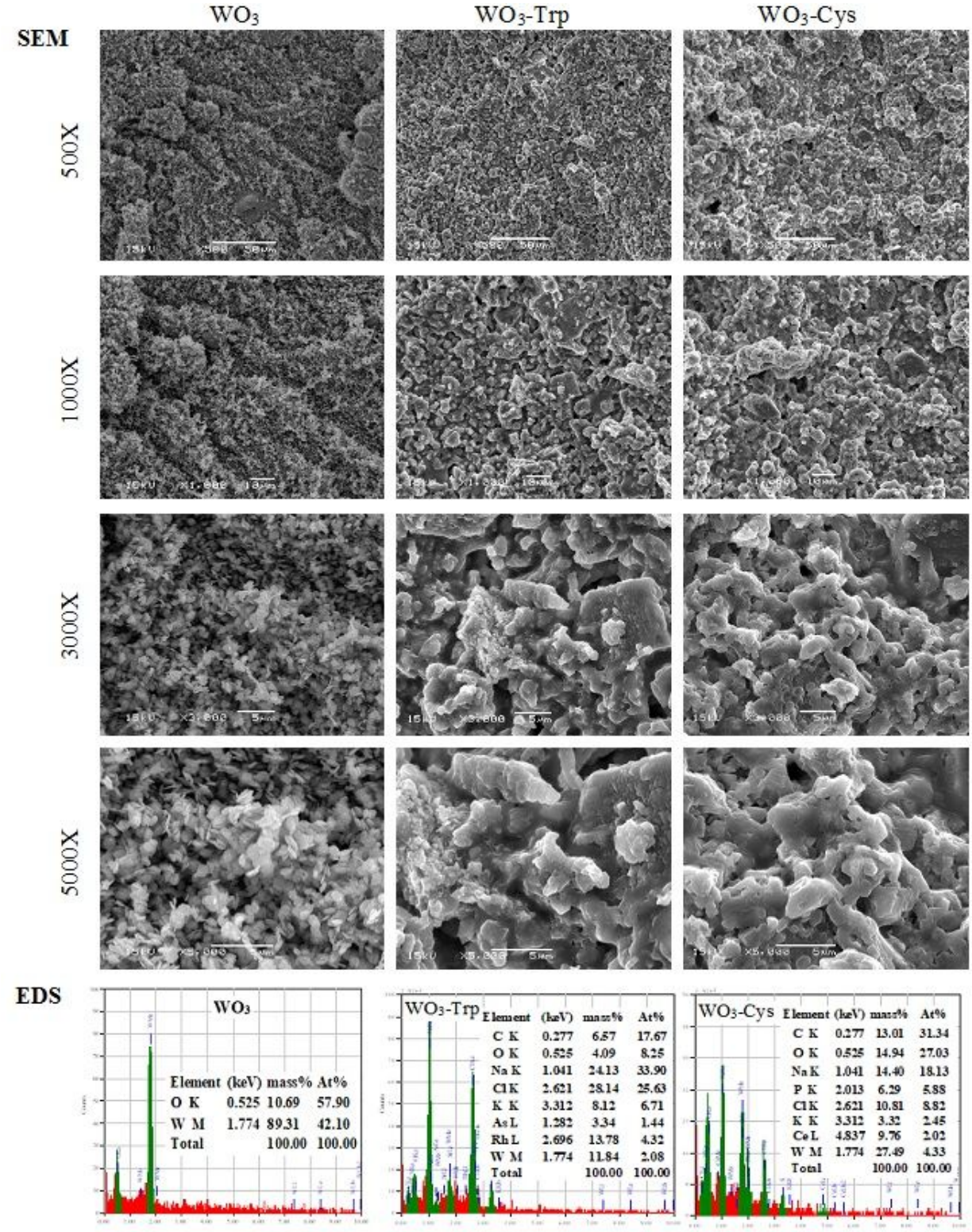

Figure 2

SEM and EDX analysis for prepared WO3 NPs (column 1), WO3-Trp (column 2) and WO3-Cys (column 3) at different magnifications.

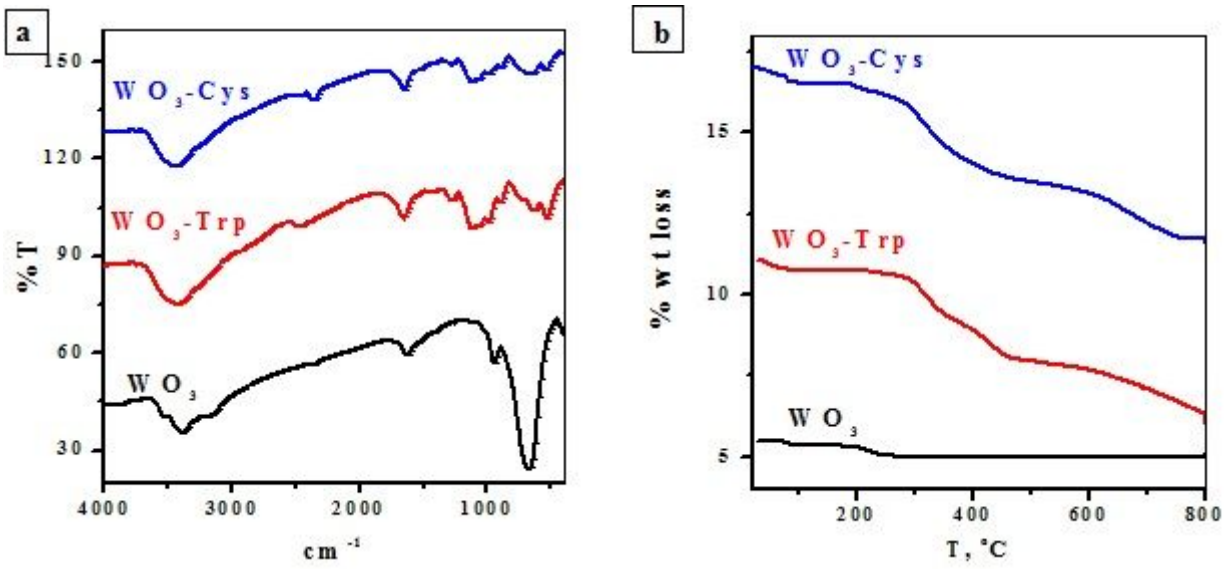

Figure 3

FT-IR spectroscopy (a) and TGA analysis (b) for prepared WO3 NPs with WO3-Trp and WO3-Cys modified NPs.

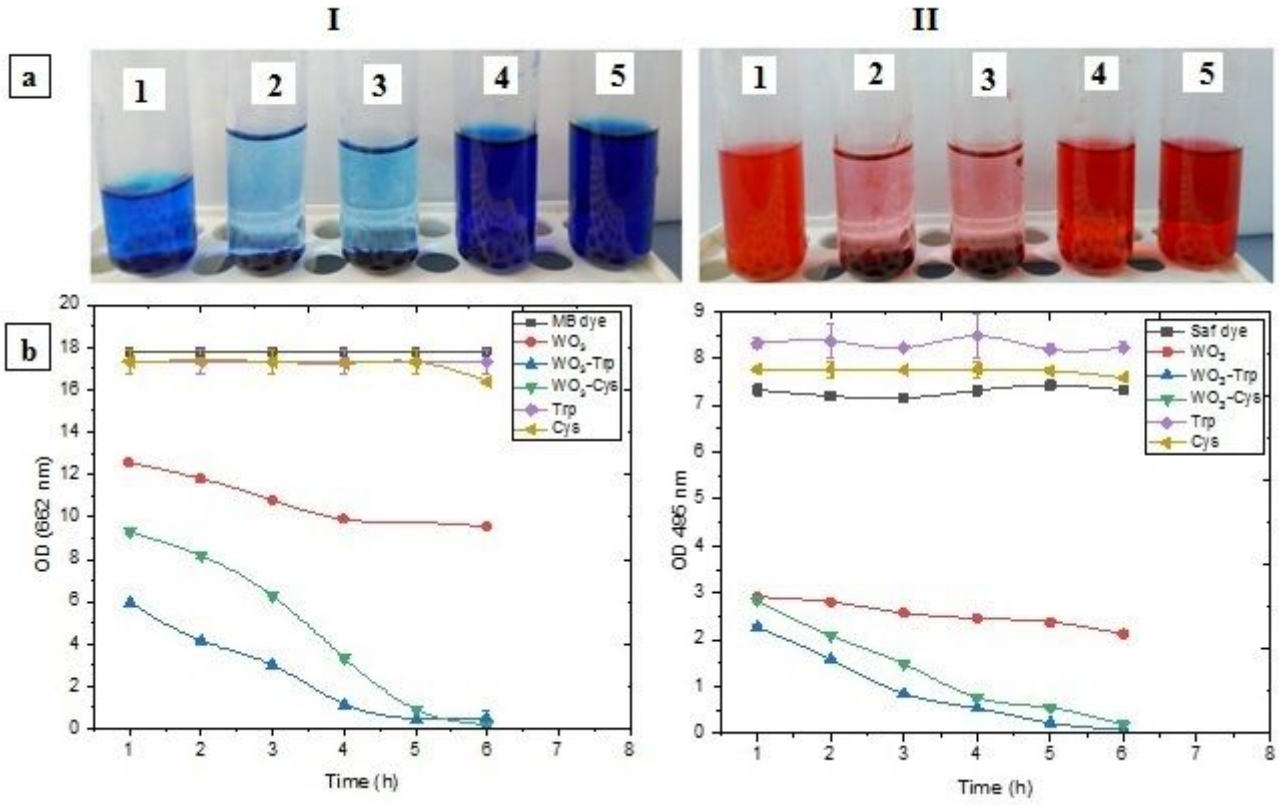

Figure 4

Photographs (a) and decolorization percentages (b) of dye removal rate for methylene blue (I) and safranin (II) by the prepared modified WO3 NPs with Trp and Cys. Methylene blue and safranin at

concentration of 100 mg/ml were decolorized by WO3 NPs (1), the modified WO3-Trp (2), WO3-Cys (3), Trp (4), and Cys (5) for 6 h.

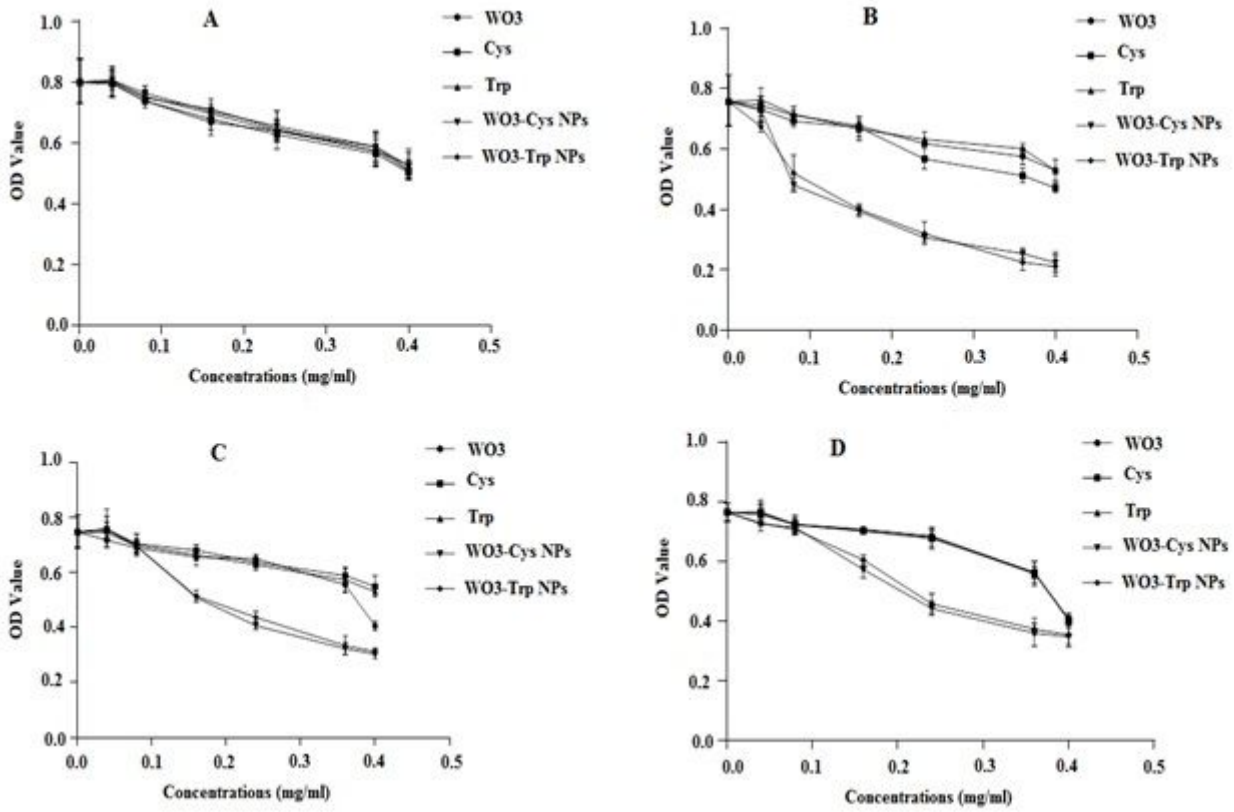

Figure 5

The dependence inhibition effect of the modified WO3 NPs on the cell viability of the normal WISH cells (A), breast cancer MCF-7 cells (B), colon cancer Caco-2 cells (C) and hepatoma HepG-2 cells (D). Both normal cells and cancer cell lines were incubated with the WO3-AAs NPs at different concentrations (0-0.5 mg/ml) for 48 h. All values are expressed as mean±SD and represent the average values from three experiments.

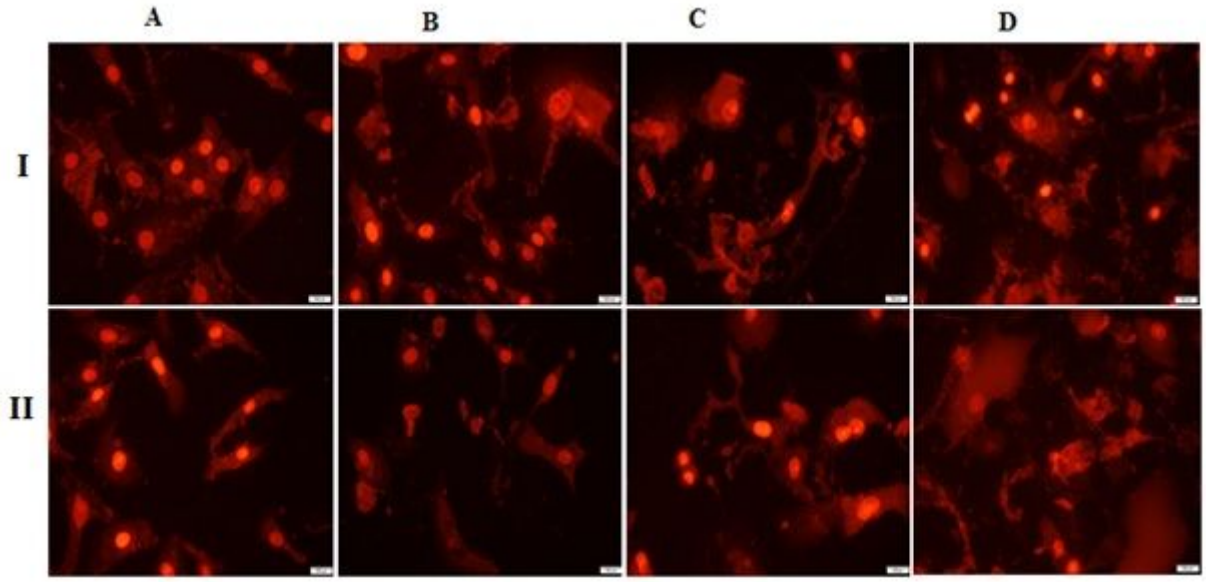

Figure 6

Fluorescence photograph of HepG-2 cells stained with PI dye under a fluorescence microscope after treatment with the modified WO3-Cys and WO3-Trp NPs (I and II, respectively). HepG-2 cells were exposed to different concentrations of 0.0, 0.1, 0.2 and 0.3 mg/ml (A, B, C and D, respectively).

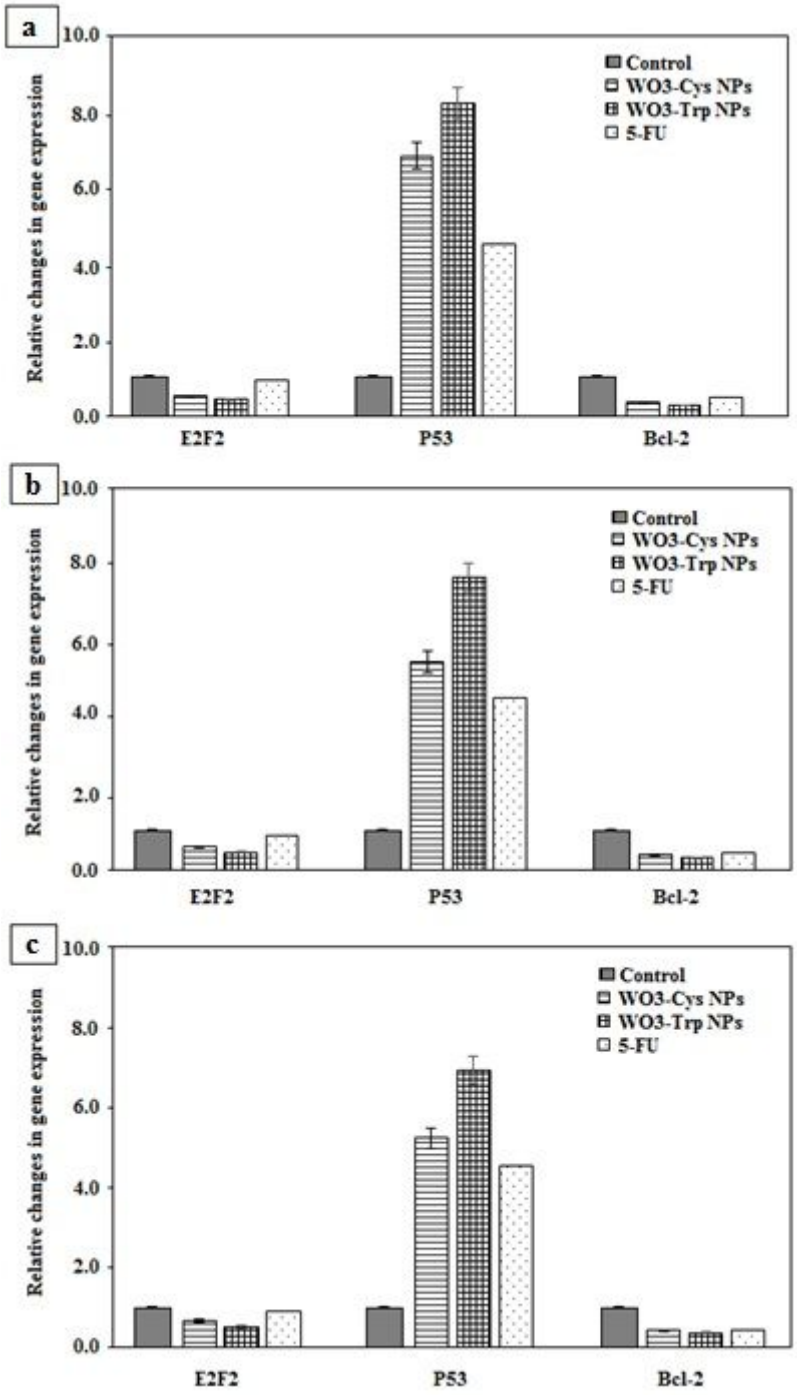

Figure 7

Effects of the modified WO3-Cys and WO3-Trp NPs on the levels of E2F2, P53 and Bcl-2 mRNA expression in MCF-7 cells (a), Caco-2 cells (b) and HepG-2 cells (c) treated with IC50 concentration of

each modified NPs and 5-FU for 48 h. The data were presented as mean ± SD and represent the average values from three experiments.

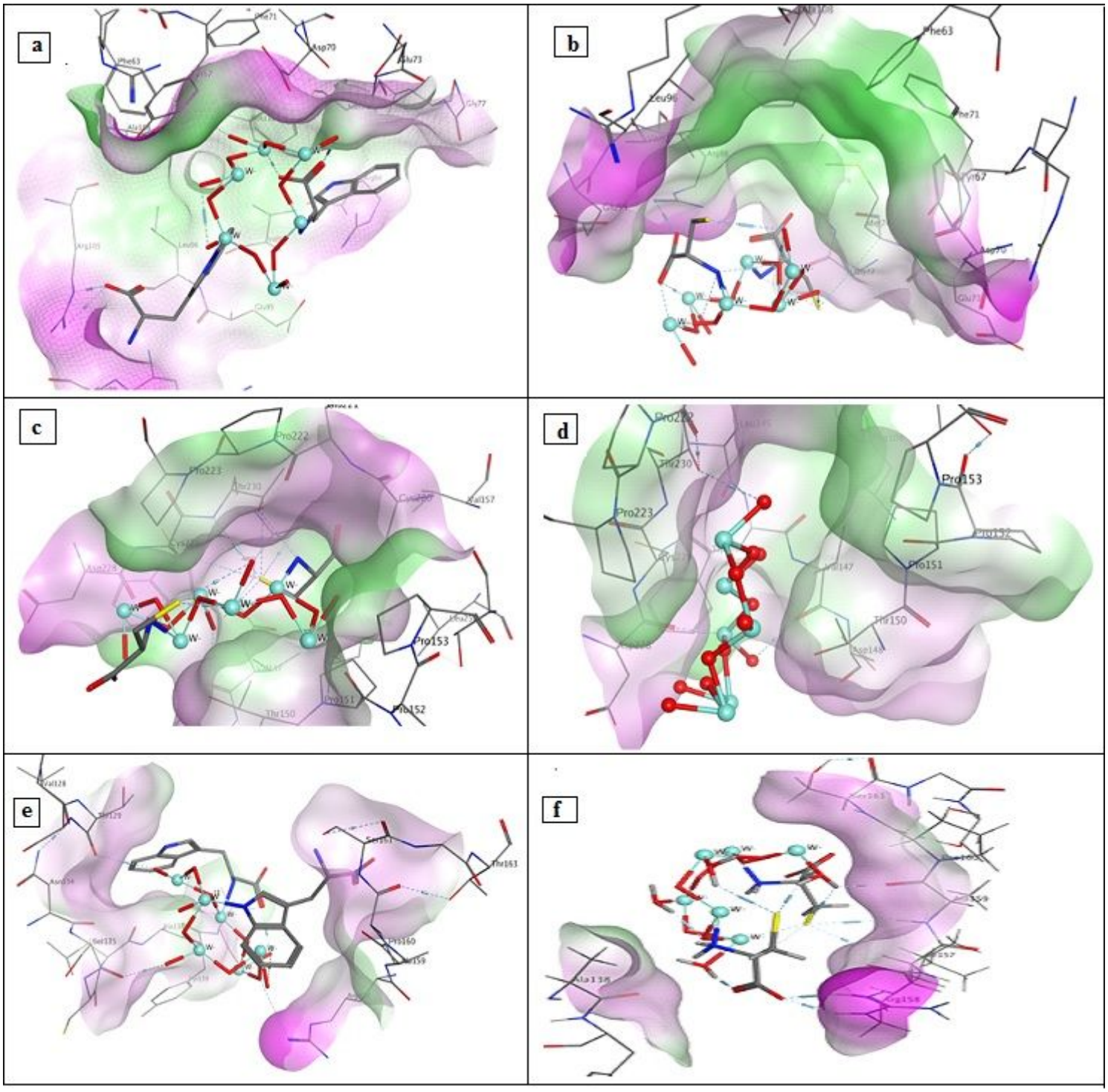

Figure 8

3D interaction of (a)WO3-Trp nanocomposite with Bcl-2 protein, (b) WO3-Cys nanocomposite with Bcl-2 protein, (c) tungestin tryptophan nanocomposite with P53 protein, (d) tungestin nanoparticle with P53 protein, (e) tungestin tryptophan nanocomposite with E2F4 protein, (f) tungestin cysteine nanocomposite with E2F4 protein.